Carbohydrate Research 569 (2026) 110074

Contents lists available at ScienceDirect

Carbohydrate Research

journal homepage: www.elsevier.com/locate/carres

Advanced structural profiling of arabinoxylans from cereal grains by high performance anion exchange chromatography with parallel pulsed amperometric and mass spectrometric detection

Lukas Sitter, Mirko Bunzel *

Institute of Applied Biosciences, Department of Food Chemistry and Phytochemistry, Karlsruhe Institute of Technology (KIT), Karlsruhe, Germany

A R T I C L E I N F O

Keywords:
Cereal grains
Dietary fiber
Arabinoxylans
Enzymatic hydrolysis
Endo-β-1,4-Xylanases
Oligosaccharide profiling

A B S T R A C T

Arabinoxylans (AX) are major hemicellulosic polysaccharides of cell walls of cereal grains. Potential health benefits and techno-functional properties of AX are determined, among others, by the extent and distribution of arabinofuranose (Ara*f*) units as substituents along the β-(1 → 4)-linked D-xylopyranose (Xyl*p*) backbone. Conventional carbohydrate analytical methods, such as methylation analysis, are time-consuming and often insufficient to capture structural diversity. Therefore, a semi-quantitative profiling method based on enzymatic AX degradation and on high-performance anion-exchange chromatography with pulsed amperometric and mass spectrometric detection (HPAEC-PAD/MS) was developed. The method relies on enzymatic depolymerization of AX in cereal dietary fiber using *endo*-β-1,4-xylanases from glycoside hydrolase families 10 and 11, releasing xylooligosaccharides (XOS) and arabinoxylooligosaccharides (AXOS), which were analyzed by HPAEC-PAD/MS. These enzyme-dependent (A)XOS profiles, which do not cover enzymatically resistant AX regions, provide indirect insights into AX structural characteristics. Newly isolated higher substituted AXOS standards were combined with commercially available compounds, resulting in 17 structurally distinct (A)XOS standards for a more detailed characterization of AX substitution patterns with Ara*f*. Furthermore, incubation conditions and chromatographic parameters were optimized, and relative response factors (RRF) of the (A)XOS standards relative to an internal standard were determined, providing a basis for routine semi-quantitative analysis. The applicability of the method was demonstrated using well-characterized cereal soluble and insoluble dietary fiber samples (five different wheat (*Triticum*) species, rye, and barley), confirming its ability to provide additional structural information on AX. Among others, it was demonstrated that the analyzed wheat species exhibited comparable (A)XOS profiles, being consistent with their close phylogenetic relationship.

1. Introduction

Cereal grains represent a major component of the human diet worldwide and are an important source of dietary fiber. In addition to providing energy and essential nutrients, whole grains have been associated with reduced risks of cardiovascular disease, type 2 diabetes, and certain gastrointestinal disorders [1,2]. These effects are largely attributed to the composition and functionality of cereal dietary fiber, which primarily reflects the structural and compositional features of cereal cell walls.

Cereal cell walls are characterized by type II primary cell walls that differ from those of dicotyledonous plants. They consist of a network of cellulose microfibrils embedded in a hydrated matrix of hemicelluloses, pectins, structural proteins, and inorganic ions. In contrast to type I primary cell walls of dicotyledons, type II primary cell walls of grasses are characterized by a markedly different polysaccharide composition. In cereals, arabinoxylans (AX) and, depending on genus and species, mixed-linked β-glucans represent the major non-cellulosic polysaccharides, whereas xyloglucans, (gluco-)mannans, and pectins occur only in minor amounts [3]. Through hydrogen bonding, AX interconnect cellulose microfibrils, forming a three-dimensional network that is essential for maintaining the mechanical stability and structural integrity of cereal cell walls.

AX consist of a β-(1 → 4)-linked D-xylopyranose (Xyl*p*) backbone substituted with α-L-arabinofuranose (Ara*f*) residues at the *O*2 and/or *O*3 positions of Xyl*p* units. A defining feature of AX is their pronounced structural heterogeneity, which arises from variations in the degree and

* Corresponding author.
E-mail address: mirko.bunzel@kit.edu (M. Bunzel).

https://doi.org/10.1016/j.carres.2026.110074
Received 10 June 2026; Received in revised form 5 August 2026; Accepted 13 August 2026
Available online 14 August 2026

Glossary

Ara*f*	arabinofuranose
AX	arabinoxylan
A/X	arabinose-to-xylose ratio
AXOS	arabinoxylooligosaccharide
DP	degree of polymerization
FID	flame ionization detection
GC	gas chromatography
GH	glycoside hydrolase
HPAEC	high performance anion exchange chromatography
IDF	insoluble dietary fiber
LOD	limit of detection
LOQ	limit of quantification
MS	mass spectrometry
PAD	pulsed amperometric detection
PMAA	partially methylated alditol acetate
RRF	relative response factor
RRT	relative retention time
SDF	soluble dietary fiber
XOS	xylooligosaccharide
XYL_{10}	*endo*-β-1,4-xylanase from GH family 10
XYL_{11}	*endo*-β-1,4-xylanase from GH family 11
Xyl*p*	xylopyranose

pattern of Ara*f* substitution across cereal species and genetics, tissue type, developmental stage, and environmental factors. The substitution patterns strongly influence intermolecular interactions and, thus, aggregation behavior and water solubility. Regions with low substitution levels can interact more readily with cellulose microfibrils, promoting aggregation and reduced solubility, whereas highly substituted AX are generally more soluble [4]. In addition, ferulic acid esterified at the *O*5 position of Ara*f* residues can form cross-links, further affecting AX extractability and cell wall architecture [5].

Enzymatic hydrolysis of AX represents an important approach to depolymerize AX into oligosaccharides, which have attracted considerable interest due to their prebiotic potential [6–9]. Recent studies further suggest that AX derived oligosaccharides may also exert stimbiotic effects by stimulating fiber-degrading microbial populations, thereby enhancing the fermentation of complex polysaccharides already present in the diet [10]. Among the enzymes involved in AX degradation, *endo*-β-1,4-xylanases are of particular importance, as they cleave the β-1,4-glycosidic bonds within the Xyl*p* backbone of AX, generating a complex mixture of linear xylooligosaccharides (XOS) and arabinoxylooligosaccharides (AXOS) that retain Ara*f* substitutions on the Xyl*p* backbone [11–13]. A nomenclature system proposed by Fauré et al. [14] is widely accepted to describe these (A)XOS. In this notation, which is used throughout this study, "X" denotes an unsubstituted Xyl*p* unit, whereas "A" refers to a Xyl*p* residue substituted with Ara*f*. Superscript numbers indicate the position of the respective Ara*f* substitution along the Xyl*p* backbone of AXOS. Product profiles following enzymatic hydrolysis are strongly influenced by enzyme specificity, particularly by the tolerance toward substitution of the AX backbone with Ara*f* near the cleavage site. Among *endo*-β-1,4-xylanases, members of the glycoside hydrolase (GH) families 10 and 11 are considered the most prominent contributors to AX depolymerization [13,15]. In contrast, GH5 xylanases have primarily been described as acting on highly substituted regions of AX, where steric hindrance limits the activity of other enzyme families [16]. GH10 xylanases preferentially cleave glycosidic linkages adjacent to mono- or disubstituted Xyl*p* residues toward the non-reducing end of AX. Their catalytic mechanism requires two consecutive unsubstituted Xyl*p* units, resulting in the formation of relatively short oligosaccharides, predominantly with a degree of polymerization (DP) of 2 - 5. Linear XOS are further degraded to dimers (X_2). Depending on the position of the Ara*f* units, A^3X, A^2XX, and $A^{2+3}XX$ represent the smallest substituted hydrolysis products [13], as a result of the fact that GH10 enzymes tolerate Ara*f* substituents at the +I subsite (different from GH11 xylanases). However, GH10 xylanases also tolerate Ara*f* substituents at the +II subsite enabling the release of oligosaccharides such as XA^2X and XA^3X with an unsubstituted non-reducing end [11]. In contrast, GH11 xylanases typically produce larger (A)XOS with DP values of 3 - 10. Because cleavage requires up to three consecutive unsubstituted Xyl*p* residues, these enzymes are usually more sensitive to substitution with Ara*f* than GH10 xylanases. GH11 xylanases characteristically produce AXOS with an unsubstituted Xyl*p* unit at the non-reducing end, extended by two Xyl*p* residues toward the reducing end. Accordingly, the AXOS backbone contains at least four Xyl*p* residues, with substitution occurring at the penultimate unit toward the non-reducing end, as illustrated by structures such as XA^3XX or $XA^{2+3}XX$. The smallest unsubstituted products released are X_2 and X_3 [11,13]. Consequently, enzymatic hydrolysis produces characteristic (A)XOS fingerprints that reflect both enzyme properties and structural features of the parent AX.

These enzyme-dependent (A)XOS profiles form the basis of enzymatic profiling approaches, which enable indirect insights into AX substitution patterns and structural organization. However, enzymatic profiling methods are usually based on a limited, often commercially available set of (A)XOS standard compounds, thereby mainly capturing the less highly substituted regions of AX [17–19]. Although they are well-developed and generally suitable for describing less-substituted AX regions, these approaches may overlook more heavily substituted regions. In a recently published study, we reported the isolation of higher substituted AXOS standard compounds from wheat flour AX using GH10 and GH11 xylanases [20]. Both enzymes were shown to be able to act on more highly substituted regions of AX, resulting in AXOS with a DP of up to 9 that contain consecutive mono- and/or disubstituted Xyl*p* units. Therefore, the aim of this study was to establish an extended semi-quantitative profiling method based on high-performance anion-exchange chromatography (HPAEC) with parallel pulsed amperometric (PAD) and mass spectrometric detection (MS) for the analysis of GH10- and GH11-derived (A)XOS from cereal dietary fiber. By using the newly isolated AXOS standard compounds, the approach enables a more detailed characterization of substitution patterns of AX with Ara*f* from different cereal sources.

2. Materials and methods

2.1. Materials and reagents

Wheat (*Triticum aestivum* L.), einkorn (*Triticum monococcum* L.), emmer (*Triticum dicoccum* Schrank ex Schübl.), spelt (*Triticum spelta*, L.), kamut (Khorasan wheat, *Triticum turgidum* subsp. *Turanicum* Á. Löve & D. Löve), rye (*Secale cereale* L.) and hulled barley (*Hordeum vulgare* L.) were either purchased as grains or as wholegrain flours from local grocery stores or online shops.

Standard compounds of isomaltotriose, laminaritriose, XOS X_2 - X_6 and AXOS A^3X, A^2XX, $A^{2+3}XX$, XA^3XX were purchased from Megazyme (Wicklow, Ireland). All other AXOS standard compounds were isolated from enzymatic digests of wheat flour arabinoxylan and completely characterized by NMR spectroscopy as described previously [20].

Ultra-pure water (Milli-Q, Millipore) was used for the preparation of aqueous solutions and chromatography eluents. Organic solvents of appropriate purity (e.g., acetone, ethanol, and dichloromethane) and methyl iodide for methylation analysis were from VWR (Darmstadt, Germany). Dimethyl sulfoxide, glacial acetic acid, sodium hydroxide

(powder), and sodium thiosulfate were purchased from Carl Roth GmbH + Co. KG (Karlsruhe, Germany). Eluents for HPAEC were prepared with sodium acetate (Honeywell Fluka), 49 - 51 % concentrated sodium hydroxide solution (ion chromatography grade, Sigma-Aldrich), and degassed water and were stored under helium pressure. Trifluoroacetic acid (suitable for high-performance liquid chromatography, purity ≥ 99.0 %) and a 1.25 M hydrochloric acid in methanol solution for monosaccharide analysis as well as 1-methylimdiazole were also obtained from Sigma-Aldrich Inc. (Darmstadt, Germany). Acetic anhydride was purchased from Honeywell Specialty Chemicals Seelze GmbH (Hannover, Germany). Deuterium oxide (99.95 % purity) for NMR measurements as well as sodium borodeuteride were from Deutero GmbH (Kastellaun, Germany).

Thermostable α-amylase (Termamyl 120 L, EC 3.2.1.1, *Bacillus licheniformis*, 120 KNU/g), protease (Alcalase 2.4 L, EC 3.4.21.62, *Bacillus licheniformis*, 2.4 AU/g), and amyloglucosidase (AMG 300 L, EC 3.2.1.3, *Aspergillus niger*, 300 AGU/g) were obtained from Novozymes (Bagsvaerd, Denmark). Recombinant GH10 *endo*-β-1,4-xylanase (XYL_{10}, EC 3.2.1.8, *Clostridium thermocellum*, Xylanase 10B, 1400 U/mL) was purchased from Nzytech (Lisboa, Portugal). Recombinant GH11 *endo*-β-1,4-xylanase (XYL_{11}, EC 3.2.1.8, *Neocallimastix patriciarum*, E-XYLNP, 10000 U/mL) was from Megazyme (Wicklow, Ireland).

2.2. Isolation of cell wall materials from cereal grains

2.2.1. Milling and defatting

Grain kernels that were not already available as whole-grain flours were milled to a particle size below 0.5 mm. The resulting or commercially available whole-grain flours were subsequently freeze-dried. The powders were then suspended in 1.5 vol of acetone (w/v) and stirred for 20 min, followed by centrifugation (4620 x g, 10 min; Multifuge X1, Fisher Scientific GmbH, Schwerte, Germany), after which the supernatant was discarded. The washing procedure was repeated three times, and the final powders were dried overnight in a drying oven at 60 °C.

2.2.2. Isolation of insoluble and soluble dietary fiber

Dried and defatted whole-grain flours, prepared as described in section 2.2.1, were used to isolate water-soluble and water-insoluble cell wall components using a slightly modified version of the method reported by Bunzel and co-workers [21]. Flour samples (30 g) were suspended in 400 mL of 0.08 M sodium phosphate buffer (pH 6.0) in a 500 mL Erlenmeyer flask. Subsequently, 3 mL of thermostable α-amylase was added, and the mixture was incubated in a water bath at 92 °C for 20 min with gentle shaking every 5 min. After incubation, the sample was cooled to room temperature in an ice bath, and the pH was adjusted to 7.5 using 1 M sodium hydroxide. Following this step, 1.4 mL of protease was added, and the mixture was incubated at 60 °C for 30 min under continuous shaking. After cooling to room temperature, the pH was adjusted to approximately 4.5 with 1 M hydrochloric acid, and 1.4 mL of amyloglucosidase was added. The solution was incubated at 60 °C for 30 min, followed by centrifugation at 4620 x g for 15 min. The supernatant was collected for the subsequent extraction of SDF, whereas the residue was retained for the isolation of IDF.

The residue was washed sequentially with four portions of 100 mL of water at 60 °C, with centrifugation following each wash, and the supernatants were combined. Subsequently, the residue was washed twice with 100 mL of 99 % ethanol and twice with 100 mL of acetone, centrifuging after each step and discarding the supernatants. The remaining solid was then dried overnight at 40 °C to yield the IDF.

Soluble dietary fiber (SDF) was recovered from the combined supernatants following enzymatic treatment and the water washes by precipitating with four volumes of 99 % ethanol overnight. The precipitate was collected by decanting the supernatant, followed by centrifugation at 4620 x g for 10 min and removal of the remaining supernatant. The residue was washed twice with 100 mL of 80 % ethanol, twice with 100 mL of 99 % ethanol, and twice with 50 mL of acetone, centrifuging after each wash and discarding the supernatants. Finally, the residue was dried at 50 °C overnight to yield the SDF.

2.3. Characterization of cell wall polysaccharides in cereal dietary fiber

2.3.1. Monosaccharide composition

To analyze the monosaccharide composition of IDF samples, 10 mg of IDF were weighed into a 4 mL vial fitted with a cap and septum, and glass beads were added. Subsequently, 150 μL of 12 M sulfuric acid was added, and the mixture was vortexed. The sample was kept in an ice bath for 30 min, with vortexing every 10 min, and then allowed to stand at room temperature for 2 h, vortexing every 30 min. After this period, the mixture was diluted with 975 μL of ultrapure water and hydrolyzed in an oven at 100 °C for 3 h [22]. The hydrolysate was cooled to room temperature, transferred using a syringe, and filtered through a 0.45 μm PTFE syringe filter (13 mm diameter, Chromafil). An aliquot of the filtrate (100 μL) was then mixed with 75 μL of 4 M sodium hydroxide and 825 μL of ultrapure water. An aliquot of this sample (10 μL) was combined with 20 μL of a 250 μM 2-deoxy-D-glucose solution as an internal standard compound (final concentration: 25 μM) and diluted with 170 μL of ultrapure water. The resulting solutions were analyzed using HPAEC-PAD.

A 1 mg/mL solution of SDF was prepared and an aliquot of 60 μL was transferred into a 1.5 mL vial and evaporated to dryness. Next, 500 μL of hydrochloric acid in 1.25 M methanol solution was added, the vial was tightly closed, and the mixture was incubated at 80 °C in a drying oven for 16 h. The mixture was then evaporated to dryness using an evaporator. Trifluoroacetic acid solution (2 M, 500 μL) was added, and the sample was incubated in a closed vial at 121 °C for 1 h [23,24]. The vial was again evaporated to dryness. To remove residual acid, 200 μL of 99 % ethanol was added twice, with each addition being evaporated to dryness. The residue was finally redissolved in 200 μL of ultrapure water. For HPAEC analysis, 20 μL of this solution was combined with 10 μL of a 250 μM 2-deoxy-D-glucose solution and 70 μL of water.

Two different systems were used for the HPAEC-PAD analysis of monosaccharides released from IDF and SDF of the different cereal species. Samples were analyzed either on an ICS-5000 system (ThermoFisher Scientific Dionex, Sunnyvale, CA, USA) equipped with a CarboPac PA-20 column (6 μm, 150 × 3 mm, ThermoFisher Scientific) or on an ALEXYS Carbohydrate Analyzer system (Antec Scientific, Alphen aan den Rijn, The Netherlands) using a SweetSep AEX200 column (5 μm, 50 × 4 mm, Antec Scientific).

For the analysis on the CarboPac PA-20 column, the flow rate was set to 0.4 mL/min, and separations were performed at 25 °C using ultrapure water (A), 0.1 M sodium hydroxide (B), and 0.1 M sodium hydroxide containing 0.5 M sodium acetate (C) as eluents. Prior to each run, the column was rinsed with 100 % B for 10 min and equilibrated with 90 % A and 10 % B for 10 min. After sample injection, the following linear gradient was applied: 0 - 1.5 min, from 90 % A to 10 % B to 97 % A and 3 % B; 1.5 - 22.0 min, isocratic at 97 % A and 3 % B; 22.0 - 27.0 min, from 97 % A to 3 % B to 100 % B; 27.1 - 37.0 min, isocratic at 60 % B and 40 % C.

For the analysis on the SweetSep AEX200 column, the flow rate was set to 0.7 mL/min, and separations were carried out at 30 °C using ultrapure water (A), 0.01 M sodium hydroxide (B), and 0.1 M sodium hydroxide containing 0.1 M sodium acetate (C). The gradient program was as follows: 0 - 12.0 min, isocratic at 60 % A and 40 % B; 12.5 - 18.0 min, from 60 % A to 40 % B to 100 % C; 18.0 - 24.0 min, isocratic at 100 % C; 24.0 - 24.5 min, from 100 % C to 60 % A and 40 % B; 24.5 - 63.5 min, isocratic at 60 % A and 40 % B.

2.3.2. Linkage composition analysis via partially methylated alditol acetates

Methylation analysis of IDF and SDF was performed according to Schendel et al. [25] with minor modifications. Samples (3 mg) were dissolved in 1 mL of dimethyl sulfoxide, and approximately 50 mg of

freshly ground sodium hydroxide was added. The mixture was incubated for 90 min in an ultrasonic bath followed by an additional 90 min at room temperature. Next, 0.5 mL of methyl iodide was added, and the reaction mixture was sonicated for 30 min, followed by incubation for another 30 min at room temperature. The solution was extracted with dichloromethane, and the organic phase was washed with 2.5 mL of 0.1 M sodium thiosulfate and twice with 1.5 mL of water. The solvent was evaporated and the samples were dried overnight in a vacuum oven at 40 °C. Hydrolysis of the methylated polysaccharides was carried out by adding 1 mL of 2 M trifluoroacetic acid and incubating at 121 °C for 90 min. After evaporation of the acid, 10 mg of sodium borodeuteride in 150 µL of 2 M aqueous ammonia was added, and reduction was performed for 60 min at room temperature before being quenched with glacial acetic acid. While cooling on ice, 225 µL of 1-methylimidazole and 1.5 mL of acetic anhydride were added, followed by incubation for 30 min at room temperature. After addition of 1.5 mL water, the mixture was extracted with 2.5 mL of dichloromethane. The organic layer was washed three times with water, and residual moisture was removed by freezing overnight at −18 °C. Partially methylated alditol acetates (PMAA) were analyzed by gas chromatography (GC) coupled to MS using GC-2010 Plus and GCMS-QP2010 SE instruments (Shimadzu, Kyoto, Japan) equipped with a DB-5 MS column (30 m × 0.25 mm i.d., 0.25 µm film thickness; Agilent Technologies, Santa Clara, CA). The oven temperature was held at 140 °C for 2 min, increased to 180 °C at 1 °C/min and held for 5 min, then ramped to 300 °C at 10 °C/min. Helium served as carrier gas at 40 cm/s. Split injection (30:1) was applied with an injector temperature of 220 °C, the transfer line temperature was 220 °C, and electron impact ionization was performed at 70 eV.

For quantification, samples were analyzed by GC (GC-2010 Plus, Shimadzu) and flame ionization detection (FID) under the same chromatographic conditions using a 10:1 split ratio. Nitrogen was used as makeup gas and the FID temperature was set to 240 °C. PMAAs were semi-quantified using molar response factors according to Sweet, Shapiro and Albersheim [26]. All analyses were performed in duplicate.

2.4. Method development

In a previous work, we reported the isolation of AXOS standard compounds from alkaline-extracted wheat flour AX [20]. The wheat flour AX was hydrolyzed using the two different *endo*-β-1,4-xylanases XYL_{10} and XYL_{11}, producing a diverse range of AXOS. These oligosaccharides were subsequently isolated and purified using a combination of chromatographic techniques and were characterized by MS and one- and two-dimensional NMR spectroscopy. In addition to the commercially available XOS and AXOS (see section 2.1) we isolated nine further AXOS from the enzymatic hydrolysates of wheat flour AX. These oligosaccharides were obtained in quantities and purities (HPAEC-PAD purity > 90 %) sufficient for their use as standard compounds. XXA^3X was excluded from method development due to its HPAEC retention behavior being identical to that of XA^3XX, whereas its abundance in hydrolysates obtained following digestion with *endo*-β-1,4-xylanases was negligible compared to XA^3XX. Consequently, eight of the isolated AXOS standard compounds were incorporated into the HPAEC-PAD profiling method, presented in this work, resulting in a total of 17 different (A)XOS standard compounds. Their structures are shown in Fig. 1.

2.4.1. HPAEC-PAD/MS analysis of (arabino-)xylooligosaccharides

HPAEC-PAD analysis of the (A)XOS was performed on an ICS-6000 system (ThermoFisher Scientific Dionex) equipped with an analytical CarboPac PA200 column (6 µm, 250 × 3 mm, ThermoFisher Scientific). The injection volume was 25 µL. A flow rate of 0.4 mL/min and a gradient composed of the following eluents were used at 25 °C: ultrapure water (A), 0.1 M sodium hydroxide (B), 0.1 M sodium hydroxide + 0.5 M sodium acetate (C). Before every run, the column was washed with 100

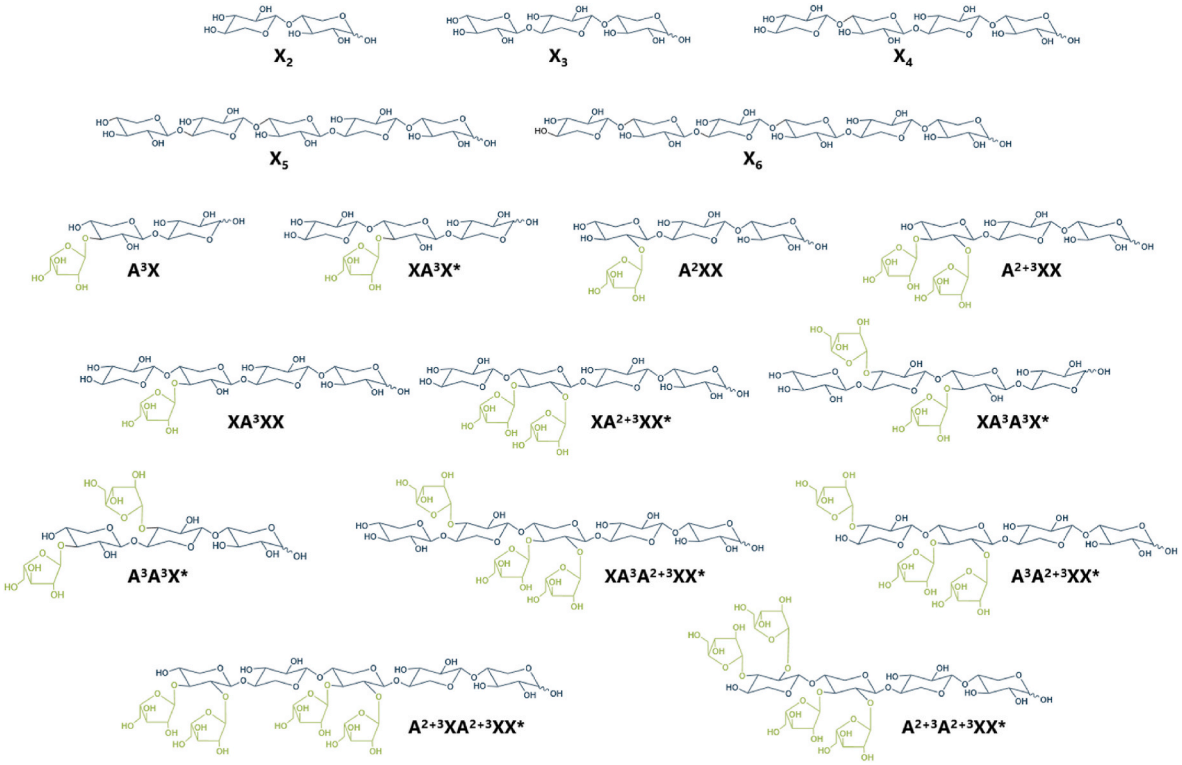

Fig. 1. Structures of xylo- and arabinoxylooligosaccharides (AXOS) included in the newly developed profiling method. Abbreviated structural names follow the nomenclature proposed by Fauré et al. [14]. Arabinofuranose units are shown in green and xylopyranose units in grey. AXOS that were isolated in a previous study are marked with an asterisk (*).

% C for 10 min and equilibrated with 90 % A and 10 % B for 20 min. After sample injection, the following linear gradient was applied for the separation of the (A)XOS: 0 - 10 min, from 90 % A to 10 % B to 40 % A, 59 % B, and 1 % C; 10.0 - 30.0 min, from 40 % A, 59 % B, and 1 % C to 40 % A, 57 % B, and 3 % C; 30.0 - 60.0 min, from 40 % A, 57 % B, and 3 % C to 27 % A, 56 % B, and 17 % C; 60.0 - 80.0 min, from 27 % A, 56 % B, and 17 % C to 17 % A, 53 % B, and 30 % C; 80.1 - 90.0 min, isocratic at 100 % C.

As an alternative to the separation on a CarboPac column, the (A)XOS can also be separated and analyzed on a SweetSep AEX200 column (see section 2.3.1) at 25 °C using the same eluents as described above and a flow rate of 0.4 mL/min: Prior to each run, the column was rinsed with 100 % B for 10 min and equilibrated with 90 % A and 10 % B for 10 min. After sample injection, the following gradient was applied: 0 - 10 min, from 90 % A to 10 % B to 45 % A, 54 % B, and 1 % C; 10.0 - 35.0 min, from 45 % A, 54 % B, and 1 % C to 25 % A, 70 % B and 5 % C; 35.0 - 80.0 min, from 25 % A, 70 % B, and 5 % C to 24 % A, 40 % B, and 36 % C; 80.1 - 90.0 min, isocratic at 100 % C.

HPAEC-PAD was further coupled with MS detection to facilitate the assignment of both known and unknown (A)XOS signals (see Supplementary Fig. 1 for details about the instrument configuration). Therefore, the eluent was split 1:2 prior to PAD detection, with the larger fraction being deionized using an electrolytically regenerated suppressor (Dionex AERS 500 with AXP pump, Thermo Fisher Scientific) against distilled water. Before entering the electrospray ionization source, a 50 μM lithium chloride solution was added to the deionized eluent (flow rate: 0.05 mL/min; Dionex AXP-MS pump, ThermoFisher Scientific) to promote the formation of characteristic lithium adducts. MS analysis was performed using a Thermo Scientific ISQ EC single quadrupole mass spectrometer equipped with a heated electrospray ionization (HESI) source (Thermo Fisher Scientific, San Jose, CA, USA). The MS was operated in positive ionization mode. The spray voltage was set to 3 kV, the capillary temperature to 250 °C, and the vaporizer temperature to 272 °C. Sheath, auxiliary, and sweep gas pressures were set to 50.8, 5.0, and 0.5 psig, respectively. The source current was 50 μA. Full-scan mass spectra were acquired over an m/z range of 150 - 1000. For more targeted and sensitive detection of (A)XOS, the instrument can also be operated in selected ion monitoring mode, monitoring the characteristic m/z values corresponding to the respective lithium adducts (see Table 1 in section 3.1.1).

2.4.2. Quantification of standard compounds by ^{1}H NMR spectroscopy

(A)XOS standard compounds were quantified using ^{1}H NMR spectroscopy, following the method by Rundlöf et al. [27]. Freeze-dried (A)XOS samples were dissolved in 550 μL of deuterium oxide containing 0.5 mg/mL acetanilide as an internal standard. ^{1}H NMR spectra were acquired using 64 scans with a relaxation delay adjusted to 15 s. The methyl signal of acetanilide (δ_H = 2.17 ppm) was used as an internal reference for the relative quantification of selected carbohydrate protons (see section 3.1.1) in the (A)XOS standard component spectra. The concentration of the (A)XOS was determined using the following equation (1):

$$c_{(A)XOS} = c_{ISt} \cdot M_{W,(A)XOS}/M_{W,ISt} \cdot n_{H,ISt}/n_{H,(A)XOS} \cdot A_{(A)XOS}/A_{ISt} \quad (1)$$

In this equation (1), $M_{W,(A)XOS}$ and $M_{W,ISt}$ denote the molecular weights of the (A)XOS analyte and the internal standard compound (ISt), respectively (g/mol). $n_{H,(A)XOS}$ and $n_{H,ISt}$ represent the number of protons giving rise to the selected NMR signals (three protons in the case of acetanilide), while $A_{(A)XOS}$ and A_{ISt} correspond to the integrated areas of the respective resonances.

2.4.3. Determination of relative response factors

From the (A)XOS standard solutions quantified by ^{1}H NMR (section 2.4.2), stock solutions with a defined concentration of 1 mM were prepared. The relative response factors (RRF) for quantification were determined using a calibration series of the respective (A)XOS at six equidistant concentration levels (0.1, 6, 12, 18, 24, and 30 μM), combined with a fixed concentration (10 μM) of the internal standard compounds isomaltotriose and laminaritriose. Due to the expected low release during enzymatic hydrolysis, the concentration range for X_5 and X_6 was adjusted to 0.1, 3, 6, 9, 12, and 15 μM. Each calibration point was analyzed in triplicate by HPAEC-PAD using the gradient described in section 2.4.1. The product of the isomaltotriose peak area and the concentration of the respective XOS or AXOS (x) was plotted against the product of the XOS or AXOS peak area and the isomaltotriose concentration (y). The slope of the resulting regression line represents the RRF of the (A)XOS. The regression lines exhibited Pearson correlation coefficients ranging from 0.99800 to 0.99999 and coefficients of variation below 10 %. To estimate both the limit of detection (LOD) and limit of quantification (LOQ), stock solutions were further diluted until signal heights corresponded to a 3- or 10-fold signal-to-noise ratio, respectively.

Table 1
Complete list of (arabino-)xylooligosaccharides ((A)XOS) included in the developed HPAEC-PAD/MS[a] profiling method, together with their relative retention times (RRT), relative response factors (RRF), molecular masses (MM), mass-to-charge ratios (m/z) and preferred lithium adducts, linear concentration ranges (CR), and limits of detection (LOD) and quantification (LOQ).

(A)XOS[b]	RRT[c]	RRF	MM/g/mol	m/z	quasi-molecular ion	CR/μM	LOD/μM	LOQ/μM
X_2	0.889^{IMT}	1.571	282	289	$[M+Li]^+$	0.1 - 30	0.01	0.05
X_3	1.069^{IMT}	1.122	414	421	$[M+Li]^+$	0.1 - 30	0.01	0.05
X_4	1.421^{IMT}	1.056	547	553	$[M+Li]^+$	0.1 - 30	0.025	0.075
X_5	1.898^{IMT}	1.041	679	685	$[M+Li]^+$	0.1 - 15	0.025	0.075
X_6	2.418^{IMT}	1.221	811	412	$[M+2{\cdot}Li]^{2+}$	0.1 - 15	0.025	0.05
A^2XX	2.677^{IMT}	1.220	547	553	$[M+Li]^+$	0.1 - 30	0.025	0.05
A^3X	2.922^{IMT}	1.691	414	421	$[M+Li]^+$	0.1 - 30	0.025	0.075
XA^3X	2.986^{IMT}	1.135	547	553	$[M+Li]^+$	0.1 - 30	0.01	0.025
XA^3XX	1.066^{LT}	1.242	679	685	$[M+Li]^+$	0.1 - 30	0.01	0.05
$XA^{2+3}XX$	1.199^{LT}	1.237	811	412	$[M+2{\cdot}Li]^{2+}$	0.1 - 30	0.01	0.05
$A^{2+3}XX$	1.217^{LT}	1.281	679	685	$[M+Li]^+$	0.1 - 30	0.025	0.05
XA^3A^3X	1.425^{LT}	1.168	811	412	$[M+2{\cdot}Li]^{2+}$	0.1 - 30	0.01	0.05
A^3A^3X	1.461^{LT}	1.478	679	685	$[M+Li]^+$	0.1 - 30	0.05	0.1
$XA^3A^{2+3}XX$	1.600^{LT}	1.005	1074	544	$[M+2{\cdot}Li]^{2+}$	0.1 - 30	0.01	0.05
$A^3A^{2+3}XX$	1.637^{LT}	1.085	942	478	$[M+2{\cdot}Li]^{2+}$	0.1 - 30	0.025	0.05
$A^{2+3}XA^{2+3}XX$	1.796^{LT}	0.845	1206	611	$[M+2{\cdot}Li]^{2+}$	0.1 - 30	0.025	0.05
$A^{2+3}A^{2+3}XX$	1.846^{LT}	1.058	1074	544	$[M+2{\cdot}Li]^{2+}$	0.1 - 30	0.025	0.05

[a] HPAEC-PAD/MS, high-performance anion-exchange chromatography with parallel pulsed amperometric and mass spectrometric detection.
[b] The nomenclature of the (A)XOS corresponds to Fauré et al. [14].
[c] RRT were determined in relation to isomaltotriose (IMT, retention time ~ 12.4 min) and laminaritriose (LT, retention time ~ 38.4 min).

2.5. Method application to cereal dietary fiber for arabinoxylan structural characterization

To obtain information about the substitution patterns of AX with Ara*f* from different cereal sources, 5 mg of IDF and SDF, respectively, were suspended/solubilized in 400 μL of ultrapure water in duplicate. Two separate incubation experiments were performed for each IDF and SDF sample using either XYL_{10} or XYL_{11}. (A)XOS were released by adding 2 μL of XYL_{10} (1400 U/mL) or 1 μL of XYL_{11} (10000 U/mL), respectively, followed by a 24-h incubation at 75 °C (XYL_{10}) and 50 °C (XYL_{11}) with continuous shaking. To terminate the enzymatic reaction, 1.6 mL of ethanol was added, precipitating also non-hydrolyzed polysaccharides within 1 h. After centrifugation (19600 x g, 10 min), an aliquot of the supernatant (500 μL) was evaporated and redissolved in ultrapure water containing 10 μM isomaltotriose and laminaritriose as internal standards. Analysis was performed by HPAEC-PAD/MS as described in section 2.4.1.

3. Results and discussion

3.1. Method development

3.1.1. Preparation of standard solutions, chromatographic conditions, and determination of relative response factors

To determine the RRF of the various (A)XOS standard compounds, stock solutions of defined concentrations were required. Due to their hygroscopic properties, gravimetric quantification of the (A)XOS was impractical. Instead, concentrations were determined by ^{1}H NMR spectroscopy with acetanilide as an internal standard (see section 2.4.2). The analytes were quantified relative to the acetanilide methyl signal ($\delta_H = 2.17$ ppm) by integrating the ^{1}H resonance signals of the (A)XOS that were most separated and could be assigned to a defined number of protons. With the exception of X_2, for which quantification was performed using the anomeric proton signal of the terminal, non-reducing Xyl*p* unit ($\delta_H = 4.45$ ppm), only the anomeric proton signals of the reducing Xyl*p* unit appeared sufficiently isolated for all XOS (X_3 - X_6). Accordingly, the sum of the integrals from the α-anomer signal ($\delta_H = 5.18$ ppm) and the β-anomer signal ($\delta_H = 4.58$ ppm) of the reducing Xyl*p* unit was used to determine their concentrations. The anomeric proton signals of the Ara*f* units within the chemical shift range of $\delta_H = 5.20$ - 5.40 ppm were suitable for quantifying the AXOS. In cases where arabinose signals were not completely separated, overlapping resonances were integrated together and the number of contributing protons was considered in the calculations (see Supplementary Table 1).

Using this information on concentrations, stock solutions and mixtures of (A)XOS were prepared to develop a suitable HPAEC based separation and quantification approach. With the developed gradient, all 17 commercially available and isolated (A)XOS standard compounds were sufficiently separated by HPAEC on a CarboPac PA200 column (see Fig. 2). Quantification of (A)XOS by HPAEC-PAD was performed using response factors relative to an internal standard. An internal standard should be structurally similar to the analytes, absent from the investigated plant materials, and compatible with the chromatographic separation of (A)XOS without causing interference. In this study, isomaltotriose proved to be a suitable internal standard for the extended profiling approach. In addition to isomaltotriose, other oligosaccharides were evaluated as potential internal standards. Laminaritriose also produced a signal clearly separated from the (A)XOS but eluted at substantially later retention times. Because retention time shifts may occur, especially during the steep acetate gradient where larger and more highly substituted AXOS elute, laminaritriose was incorporated as an additional internal standard for identification of the analytes based on relative retention times (RRT).

While the XOS elute before the AXOS and in ascending order of their DP, the retention behavior of the AXOS depends both on the length of the Xyl*p* backbone and on the number and position of Ara*f* substituents. The elution order of commercially available (A)XOS standard compounds is consistent with that reported in other studies [18,19,28,29]. In addition, it is noticeable that structurally similar AXOS, such as $XA^{2+3}XX$ and $A^{2+3}XX$ or XA^3A^3X and A^3A^3X, each elute in pairs within close temporal proximity. Furthermore, for larger AXOS with a DP > 6, an increasing broadening of the peak shape is observed after approximately 60 min, eventually leading to the formation of double peaks (see signals of $A^{2+3}XA^{2+3}XX$ and $A^{2+3}A^{2+3}XX$ in Fig. 2). Mass spectrometric analysis showed that these are likely hydrolysis products formed during chromatographic separation. Accordingly, the mass spectrum of $A^{2+3}XA^{2+3}XX$ is dominated by the doubly lithium-adducted ion ($[M+2{\cdot}Li]^{2+}$) at *m/z* 611, representing nine pentose units, while a less intense signal at *m/z* 544 ($[M+2{\cdot}Li]^{2+}$) is also observed, corresponding to an AXOS with eight pentose units. Given that late-eluting AXOS are

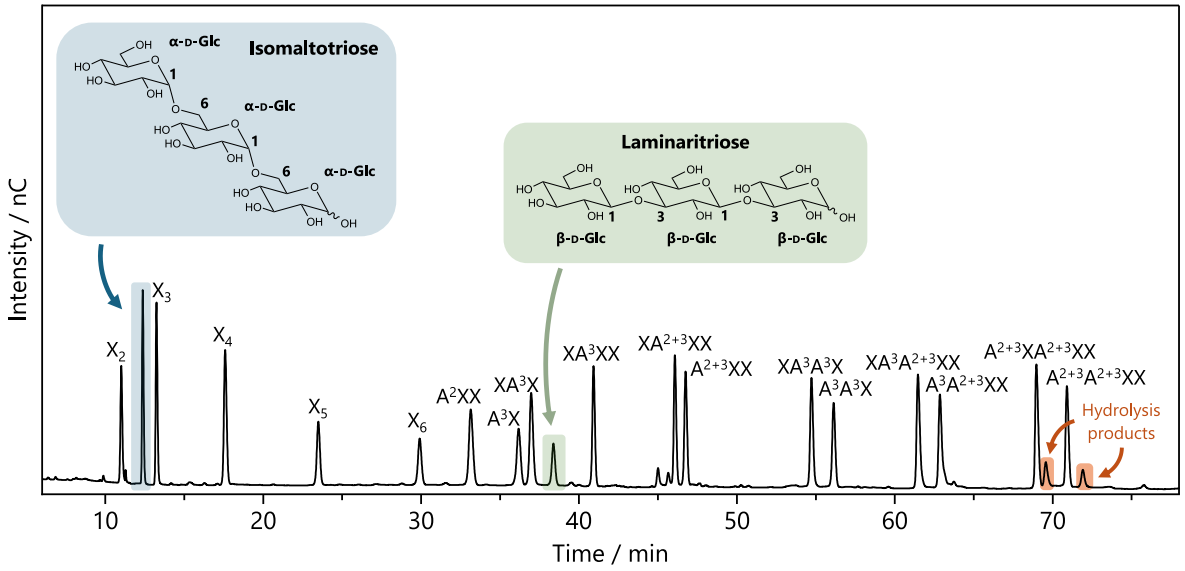

Fig. 2. Separation of commercially available and isolated (arabino-)xylooligosaccharides ((A)XOS) and internal standard compounds (structures of isomaltotriose and laminaritriose shown in blue and green, respectively) by high performance anion exchange chromatography with pulsed amperometric detection. Hydrolysis products of AXOS resulting from alkaline peeling that were included in the determination of relative response factors are highlighted in red. The nomenclature of the (A)XOS standard compounds is taken from the naming system according to Fauré et al. [14]. Glc, glucose.

exposed to strongly alkaline conditions for extended periods of time during HPAEC separation, alkaline peeling is a plausible explanation for the observed degradation and its influence on retention behavior. This process involves the stepwise cleavage of the Xyl*p* backbone from the reducing end under alkaline conditions, leading to the release of monomeric xylose units [30]. Nevertheless, when determining the RRF of these AXOS standards, the signals of hydrolytic degradation products were consistently included during peak integration. Furthermore, other (A)XOS standards were also carefully evaluated for potential alkaline degradation. No interference of possible degradation products with the quantification of other (A)XOS standards was detected. Therefore, alkaline degradation products did not affect the quantitative analysis under the applied experimental conditions.

Table 1 summarizes the determined RRF values as well as additional validation parameters of the developed HPAEC-PAD/MS profiling method. The concentration of (A)XOS in aqueous solution can be calculated using the following equation (2):

$$c_{(A)XOS} = RRF \cdot c_{IMT} \cdot A_{(A)XOS}/A_{IMT} \quad (2)$$

Here, $c_{(A)XOS}$ and c_{IMT} denote the concentrations, while $A_{(A)XOS}$ and A_{IMT} represent the corresponding peak areas of (A)XOS and isomaltotriose, respectively. The application of RRFs is limited to the defined linear concentration range of the (A)XOS (0.1 - 30.0 μM). Consequently, samples exceeding this range require appropriate dilution. The RRFs eliminate the need for external calibration and reference standards, thereby reducing analytical workload. Under identical chromatographic conditions, they are expected to be transferable across comparable HPAEC systems. Using the developed profiling method, (A)XOS can be reliably detected and quantified down to a concentration range of approximately 10 - 50 nM. The resulting LOD and LOQ values are in good agreement with those reported in the literature for commercially available (A)XOS [18,19]. RRT, calculated from the ratio of (A)XOS to internal standard retention times, were primarily used for compound identification (see Table 1). Early-eluting (A)XOS were referenced to isomaltotriose, whereas later-eluting AXOS were referenced to laminaritriose. RRT are more stable against variations in mobile phase composition and temporal changes in eluent conditions as compared to absolute retention times. Thus, by using RRT and RRF the method is also applicable in other laboratories. In addition, the routine HPAEC-PAD method was further coupled with parallel MS detection (see Supplementary Fig. 1) to enable efficient characterization of liberated (A)XOS. The eluent stream was split and simultaneously directed to the PAD and the mass spectrometer. For MS detection, efficient desalting was achieved using an upstream suppressor, which removed the majority of eluent salts prior to ionization. After desalting, lithium chloride was introduced to promote the formation of stable lithium adducts during electrospray ionization. Detection of (A)XOS as lithium adducts eliminates the need for routine assignment based on reference standards once the method has been established. Instead, released (A)XOS can be reliably identified using their characteristic *m/z* values in combination with RRT (see Table 1). Moreover, the combined HPAEC-PAD/MS approach enables an initial assessment of unknown or potentially co-eluting (A)XOS signals and supports the detection of additional oligomeric species beyond those covered by the available standards. The coupling of HPAEC-PAD with MS detection has previously been successfully demonstrated in our group for the analysis of, for example, xyloglucan oligosaccharides [31].

In addition to the CarboPac-200 column (ThermoFisher Scientific), a SweetSep-AEX200 column (Antec Scientific) was also tested for the chromatographic separation of the (A)XOS standard compounds. Initially, the same mobile phase compositions were employed. However, the elution capacity of the previously developed gradient was too weak, particularly for the elution of the more highly substituted AXOS. Thus, higher proportions of sodium hydroxide and a steeper acetate gradient were used (see section 2.4.1). Finally, using the SweetSep-AEX-200 column, a complete separation of the (A)XOS as well as the internal standard compounds isomaltotriose and laminaritriose was achieved in analysis times comparable to those of the CarboPac-200 column (see Supplementary Fig. 2). Also, the elution order of the (A)XOS corresponded to that observed on the CarboPAC-200 column. Furthermore, the applicability of the determined RRF (see Table 1) for the quantification of (A)XOS on the SweetSep-AEX200 was evaluated. For this purpose, mixtures of (A)XOS at various concentrations, corresponding to those used for RRF determination (see section 2.4.3), were analyzed. With few exceptions, the deviation between theoretical and experimentally determined (A)XOS concentrations was within ± 10 %. Therefore, RRFs are also suitable for quantifying (A)XOS on the SweetSep-AEX200. All additional parameters, including RRT as well as the LOD and LOQ values of the (A)XOS, are provided in the supplementary material (see Supplementary Table 2).

3.2. Sample preparation and enzymatic digestion using XYL_{10} and XYL_{11}

Within the cereal cell wall matrix, only specific AX structures are accessible to enzymatic hydrolysis by *endo*-β-1,4-xylanases of glycoside hydrolase families 10 and 11. The proportion of AX available for subsequent depolymerization is therefore highly dependent on the employed extraction strategy, including the preparation of intact cell wall material, IDF and SDF fractions, or alkaline hemicellulosic extracts. In the present work, both IDF and SDF were employed, thereby closely resembling typical dietary fiber preparations derived from cereal samples. This approach ensures the applicability of the method to fiber-rich samples from cereal-based food sources. As discussed in more detail below, the sample preparation protocol must effectively eliminate any endogenous free oligosaccharides present in the plant material. Moreover, enzymes capable of generating additional oligosaccharides during or after extraction, as well as throughout the controlled enzymatic hydrolysis step, must be fully inactivated.

The incubation conditions for the enzymatic hydrolysis of IDF and SDF using XYL_{10} and XYL_{11} (see section 2.5) were selected based on those previously established for the preparative isolation of AXOS standard compounds from wheat flour AX [20]. To avoid adverse effects on ion chromatography caused by the presence of additional buffer salts, enzymatic digestions were generally carried out in water [32]. In addition, the influence of incubation time on the release of (A)XOS from rye-derived IDF and SDF was investigated. A 24-h incubation period was selected to achieve complete enzymatic degradation of the accessible AX domains and maximize the release of soluble (A)XOS products. Enzyme inactivation was evaluated by adding ethanol to solutions of XYL_{10} and XYL_{11} to final concentrations of 50, 60, 70, or 80 % (v/v). Following removal of ethanol by evaporation, residual enzymatic activity was assessed by incubating the treated enzyme solutions with wheat flour AX and comparing the resulting hydrolysis products with those obtained using untreated enzyme solutions. No residual enzymatic activity was detected after treatment with 50 % ethanol (v/v). Nevertheless, a final ethanol concentration of 80 % (v/v) was used in the analytical procedure to ensure efficient precipitation of high-molecular-weight water-soluble components. This step was primarily implemented to protect the HPAEC system from potential contamination. Importantly, neither the total amount nor the relative distribution of (A)XOS with a DP < 9 in the low-molecular-weight soluble fraction of the hydrolysate was affected by this procedure. Thus, the evaporated supernatant can subsequently be directly analyzed after the addition of the internal standards isomaltotriose and laminaritriose.

As already mentioned above, the developed profiling method exclusively captures AX structures that are susceptible to hydrolysis by *endo*-β-1,4-xylanases of glycosyl hydrolase families 10 and 11. Consequently, highly Ara*f*-substituted AX domains, which are sterically and structurally less accessible to these enzymes, are not adequately represented in the analysis. In addition, not only the degree of substitution with Ara*f* units but also other cell-wall-related modifications influence

enzymatic accessibility. In particular, acetylation as well as ferulic acid-mediated cross-linking can further stabilize the AX structure and thereby significantly reduce its susceptibility to xylanase-catalyzed hydrolysis. However, both XYL_{10} and XYL_{11} are capable of releasing feruloylated AXOS from cereal dietary fiber. Under the strongly alkaline conditions of HPAEC, ester-linked ferulic acid and acetyl groups are cleaved, resulting in the detection of these structures exclusively in their de-esterified forms. Hydrolysis products with a DP > 9 may be present in the hydrolysates. However, due to their long retention times, they are not captured within the chromatographic time window of the profiling method.

For the profiling of (A)XOS released following separate hydrolysis of AX with either XYL_{10} or XYL_{11}, isolated cell wall-derived materials such as dietary fiber or non-starch polysaccharide fractions are generally suitable as starting substrates. In some cases, chromatographic analyses of untreated control samples (i.e., without incubation with XYL_{10}/XYL_{11}) still revealed low levels of free mono-, di-, or oligosaccharides. These were particularly observed in SDF preparations. Such background signals may complicate the clear assignment and quantification of (A)XOS generated by enzymatic hydrolysis with XYL_{10} and XYL_{11}. Therefore, the use of appropriate controls, including enzyme-free or enzyme-inactivated samples, is essential. In addition, a rigorous and standardized sample preparation is required, including thorough washing steps to remove residual sugars originating from starch degradation as well as naturally occurring low-molecular-weight carbohydrates (see section 2.2.2).

3.3. Method application on cereal samples

The developed profiling method was applied to investigate substitution of AX with Ara*f* units, using different cereal sources such as wheat (*Triticum aestivum* L.), einkorn (*Triticum monococcum* L.), emmer (*Triticum dicoccum* Schrank ex Schübl.), spelt (*Triticum spelta*, L.), kamut (khorasan wheat, *Triticum turgidum* subsp. *Turanicum* Á. Löve & D. Löve), rye (*Secale cereale* L.), and hulled barley (*Hordeum vulgare* L.). Applying the determined RRF (section 3.1.1), the molar concentrations and relative composition of (A)XOS released from IDF (see Table 2) and SDF (see Table 3) by enzymatic hydrolysis with XYL_{10} and XYL_{11} were determined. Only rarely and only for individual (A)XOS components, the range/2 from duplicate measurements exceeded 10 %, supporting the overall acceptable precision of the profiling method. For improved visualization, the data are additionally presented as bar graphs in the Supplementary Material (see Supplementary Fig. 3).

The amounts of (A)XOS released by XYL_{10} ranged from 40.3 to 295.9 μmol/g for IDF samples and from 19.5 to 255.7 μmol/g for SDF samples. Corresponding values for XYL_{11} ranged from 13.7 to 252.9 μmol/g for IDF samples and from 7.1 to 65.3 μmol/g for SDF samples. The results demonstrate that the enzymatic accessibility of AX depends not only on the cereal source but also on whether the AX are soluble or insoluble (the former likely being more heavily substituted and therefore less accessible to enzyme treatment), as well as on the xylanase used for hydrolysis. In particular, water-soluble AX were hydrolyzed more efficiently by XYL_{10} than by XYL_{11}, as XYL_{10} requires only two consecutive unsubstituted Xyl*p* residues for cleavage, whereas XYL_{11} requires three, resulting in a greater number of potential cleavage sites for XYL_{10} [13,15].

Analysis of the relative (A)XOS composition in XYL_{10}-and XYL_{11}-derived hydrolysates of wheat dietary fiber revealed comparable ratios of total XOS and AXOS released from IDF and SDF by both enzymes. Hydrolysis of IDF predominantly produced XOS (71.0 mol% with XYL_{10}; 76.9 mol% with XYL_{11}), whereas AXOS dominated in SDF hydrolysates (65.6 mol% and 59.8 mol%, respectively). These findings indicate extended unsubstituted Xyl*p* regions in AX from IDF, while AX in SDF are more highly substituted with arabinose, likely contributing to increased water solubility.

X_2 was the most abundant XOS, followed by X_3. In the XYL_{11}

Table 2
Relative composition (mol% ± range/2, n = 2) of enzymatically released (arabino-)xylooligosaccharides ((A)XOS) from cereal insoluble dietary fibers (IDF) using *endo*-β-1,4-xylanases from glycoside hydrolase families 10 (XYL_{10}) and 11 (XYL_{11}).

(A)XOS[a]	wheat IDF		einkorn IDF		emmer IDF		kamut IDF		spelt IDF		rye IDF		barley IDF	
	XYL_{10}	XYL_{11}	XYL_{10}	XYL_{11}	XYL_{10}	XYL_{11}	XYL_{10}	XYL_{11}	XYL_{10}	XYL_{11}	XYL_{10}	XYL_{11}	XYL_{10}	XYL_{11}
X_2	52.3 ± 1.5	44.5 ± 0.5	47.8 ± 0.7	54.7 ± 4.3	42.0 ± 1.5	47.3 ± 1.2	43.0 ± 0.2	46.5 ± 0.6	52.8 ± 2.5	62.8 ± 1.8	51.7 ± 1.2	67.4 ± 0.8	24.5 ± 0.1	43.5 ± 0.5
X_3	18.0 ± 2.4	25.5 ± 0.1	17.5 ± 0.1	16.8 ± 4.9	25.9 ± 0.0	27.4 ± 0.9	18.0 ± 0.5	24.0 ± 0.3	14.2 ± 1.9	9.9 ± 1.7	16.9 ± 0.5	3.8 ± 0.6	7.7 ± 0.3	5.7 ± 0.6
X_4	0.7 ± 0.2	5.2 ± 0.1	-	6.3 ± 0.2	4.6 ± 0.7	7.2 ± 0.4	1.0 ± 0.2	5.2 ± 0.0	-	6.4 ± 0.3	0.5 ± 0.1	7.2 ± 0.2	-	-
X_5	-	1.1 ± 0.0	-	1.3 ± 0.0	-	1.4 ± 0.1	-	1.0 ± 0.0	-	1.1 ± 0.1	-	1.3 ± 0.0	-	-
X_6	-	0.6 ± 0.0	-	0.8 ± 0.0	-	0.8 ± 0.0	-	0.5 ± 0.0	-	0.7 ± 0.0	-	0.9 ± 0.0	-	-
A^2X	0.8 ± 0.0	-	0.7 ± 0.1	-	-	-	0.9 ± 0.0	-	0.9 ± 0.0	-	0.7 ± 0.1	-	2.6 ± 0.2	-
A^3X	6.3 ± 0.5	-	7.9 ± 0.2	-	4.6 ± 0.0	0.4 ± 0.0	8.7 ± 0.1	0.2 ± 0.0	4.8 ± 0.0	-	8.9 ± 0.1	0.3 ± 0.0	11.9 ± 0.2	-
XA^3X	7.6 ± 0.4	0.6 ± 0.0	9.2 ± 0.1	0.6 ± 0.1	7.5 ± 0.1	0.3 ± 0.0	9.8 ± 0.0	0.6 ± 0.0	7.4 ± 0.1	0.5 ± 0.0	9.3 ± 0.0	0.4 ± 0.0	10.0 ± 0.1	-
XA^3XX	0.6 ± 0.2	14.9 ± 0.2	0.9 ± 0.0	13.5 ± 0.4	-	10.1 ± 0.0	-	13.9 ± 0.2	-	11.5 ± 0.2	0.8 ± 0.1	15.3 ± 0.3	0.4 ± 0.0	17.4 ± 0.6
$XA^{2+3}XX$	4.3 ± 0.0	5.8 ± 0.5	3.7 ± 0.0	4.4 ± 0.2	5.3 ± 0.3	4.3 ± 0.1	14.1 ± 0.1	5.9 ± 0.1	5.7 ± 0.1	5.7 ± 0.3	1.5 ± 0.0	1.9 ± 0.1	12.1 ± 0.2	32.4 ± 0.9
$A^{2+3}XX$	3.3 ± 0.1	-	3.1 ± 0.0	-	3.5 ± 0.1	-	10.9 ± 0.0	0.2 ± 0.0	5.2 ± 0.2	-	1.2 ± 0.0	0.3 ± 0.0	15.2 ± 0.1	-
XA^3A^3X	1.2 ± 0.1	0.6 ± 0.0	1.7 ± 0.1	0.5 ± 0.0	1.4 ± 0.0	0.3 ± 0.0	2.6 ± 0.0	0.5 ± 0.0	1.5 ± 0.0	0.4 ± 0.0	2.5 ± 0.1	0.9 ± 0.0	2.1 ± 0.0	-
A^3A^3X	1.8 ± 0.1	-	2.7 ± 0.1	-	2.1 ± 0.0	-	3.5 ± 0.0	-	2.4 ± 0.0	-	4.1 ± 0.1	-	3.6 ± 0.1	-
$XA^3A^{2+3}XX$	0.5 ± 0.0	1.2 ± 0.1	0.7 ± 0.0	1.1 ± 0.1	-	0.4 ± 0.0	3.3 ± 0.0	1.2 ± 0.0	0.9 ± 0.0	1.0 ± 0.1	0.2 ± 0.0	0.3 ± 0.0	1.4 ± 0.0	7.7 ± 0.2
$A^3A^{2+3}XX$	0.7 ± 0.1	-	1.1 ± 0.0	-	0.3 ± 0.0	-	3.4 ± 0.0	0.3 ± 0.0	1.0 ± 0.0	-	0.3 ± 0.0	-	1.3 ± 0.0	-
$A^{2+3}XA^{2+3}XX$	0.8 ± 0.0	-	1.0 ± 0.0	-	1.2 ± 0.1	-	3.7 ± 0.0	-	1.2 ± 0.0	-	0.5 ± 0.0	-	3.7 ± 0.0	6.1 ± 0.1
$A^{2+3}A^{2+3}XX$	1.1 ± 0.0	-	1.9 ± 0.1	-	1.6 ± 0.1	-	5.6 ± 0.0	-	1.9 ± 0.0	-	0.9 ± 0.0	-	3.6 ± 0.0	-

[a] The nomenclature of the (A)XOS corresponds to Fauré et al. [14].

Table 3
Relative composition (mol% ± range/2, n = 2) of enzymatically released (arabino-)xylooligosaccharides ((A)XOS) from cereal soluble dietary fibers (SDF) using *endo*-β-1,4-xylanases from glycoside hydrolase families 10 (XYL_{10}) and 11 (XYL_{11}).

(A)XOS[a]	wheat SDF		einkorn SDF		emmer SDF		kamut SDF		spelt SDF		rye SDF		barley SDF	
	XYL_{10}	XYL_{11}	XYL_{10}	XYL_{11}	XYL_{10}	XYL_{11}	XYL_{10}	XYL_{11}	XYL_{10}	XYL_{11}	XYL_{10}	XYL_{11}	XYL_{10}	XYL_{11}
X_2	29.2 ± 0.4	27.7 ± 1.0	26.9 ± 0.5	29.2 ± 1.0	22.6 ± 0.1	27.8 ± 0.2	28.8 ± 0.3	27.0 ± 0.5	52.8 ± 2.5	43.0 ± 2.0	19.2 ± 0.0	20.0 ± 0.2	23.4 ± 0.5	28.1 ± 0.1
X_3	5.2 ± 0.5	12.5 ± 0.5	4.2 ± 0.2	9.2 ± 0.5	4.4 ± 0.1	9.8 ± 0.6	4.7 ± 0.3	11.4 ± 0.0	14.2 ± 1.9	-	5.6 ± 0.1	9.8 ± 0.3	2.6 ± 0.1	8.4 ± 0.5
X_4	-	-	-	-	-	-	-	-	-	-	-	1.0 ± 0.0	-	-
X_5	-	-	-	-	-	-	-	-	-	-	-	-	-	-
X_6	-	-	-	-	-	-	-	-	-	-	-	-	-	-
A^2XX	0.9 ± 0.1	-	0.8 ± 0.0	-	1.2 ± 0.0	-	0.9 ± 0.0	-	1.1 ± 0.0	-	0.5 ± 0.0	-	4.7 ± 0.5	-
A^3X	9.6 ± 0.0	-	10.5 ± 0.1	-	4.8 ± 0.0	-	8.7 ± 0.1	-	8.0 ± 0.4	-	15.5 ± 0.2	-	6.3 ± 0.0	-
XA^3X	11.6 ± 0.4	4.2 ± 0.2	10.7 ± 0.0	3.2 ± 0.9	6.3 ± 0.0	2.9 ± 0.1	9.8 ± 0.0	1.6 ± 0.0	10.4 ± 0.2	1.8 ± 0.0	13.5 ± 0.0	4.2 ± 0.1	6.3 ± 0.1	-
XA^3XX	0.4 ± 0.1	28.4 ± 0.5	0.3 ± 0.0	27.1 ± 0.4	0.4 ± 0.0	15.3 ± 0.2	-	24.3 ± 0.1	1.6 ± 0.4	20.2 ± 0.5	3.3 ± 0.2	45.2 ± 0.1	-	17.4 ± 0.6
$XA^{2+3}XX$	13.9 ± 0.1	20.1 ± 0.1	11.6 ± 0.0	21.3 ± 0.7	18.8 ± 0.1	33.3 ± 0.4	14.1 ± 0.1	21.6 ± 0.0	14.6 ± 0.4	21.2 ± 1.1	3.1 ± 0.1	8.5 ± 0.0	16.9 ± 0.2	32.4 ± 0.9
$A^{2+3}XX$	10.1 ± 0.0	-	9.4 ± 0.0	-	15.5 ± 0.0	-	10.9 ± 0.0	-	10.1 ± 0.5	-	2.8 ± 0.1	-	17.1 ± 0.1	-
XA^3A^3X	2.3 ± 0.0	-	3.6 ± 0.0	1.5 ± 0.3	1.5 ± 0.0	1.4 ± 0.0	2.6 ± 0.0	1.4 ± 0.0	1.9 ± 0.1	3.6 ± 0.1	10.1 ± 0.0	6.5 ± 0.0	1.2 ± 0.1	-
A^3A^3X	2.3 ± 0.0	-	4.4 ± 0.0	-	1.4 ± 0.0	-	3.5 ± 0.0	-	2.6 ± 0.1	-	13.9 ± 0.1	-	1.9 ± 0.2	-
$XA^3A^{2+3}XX$	3.8 ± 0.1	7.1 ± 0.1	4.2 ± 0.0	8.5 ± 0.3	3.6 ± 0.0	9.5 ± 1.3	3.3 ± 0.0	6.9 ± 0.1	3.6 ± 0.1	5.6 ± 0.3	1.6 ± 0.0	4.7 ± 0.0	4.8 ± 0.1	7.7 ± 0.2
$A^3A^{2+3}XX$	4.0 ± 0.0	-	4.7 ± 0.0	-	3.4 ± 0.0	-	3.4 ± 0.0	-	3.1 ± 0.1	-	2.8 ± 0.1	-	4.6 ± 0.5	-
$A^{2+3}XA^{2+3}XX$	2.9 ± 0.0	-	3.4 ± 0.1	-	6.9 ± 0.1	-	3.7 ± 0.0	5.9 ± 0.1	3.7 ± 0.1	4.6 ± 0.1	3.1 ± 0.0	-	5.1 ± 0.2	6.1 ± 0.1
$A^{2+3}A^{2+3}XX$	3.8 ± 0.0	-	5.3 ± 0.0	-	9.2 ± 0.0	-	5.6 ± 0.0	-	3.6 ± 0.1	-	5.1 ± 0.0	-	5.1 ± 0.1	-

[a] The nomenclature of the (A)XOS corresponds to Fauré et al. [14].

hydrolysate of wheat IDF, additional amounts of X_4 (5.2 mol%) and minor levels of X_5 and X_6 (~1 mol%) were detected. The structural diversity of AXOS was substantially greater after XYL_{10} hydrolysis, with all AXOS, including more complex structures (DP > 7), quantified in both IDF and SDF hydrolysates. In contrast, among these higher-substituted AXOS, only $XA^3A^{2+3}XX$ was detected in the XYL_{11} hydrolysates (wheat IDF: 1.2 mol%, wheat SDF: 7.1 mol%). This is likely due to the fact that GH10 xylanases can use more cleavage sites for the hydrolysis of the Xyl*p* backbone. Accordingly, only two consecutive unsubstituted Xyl*p* units are required for cleavage by XYL_{10}, whereas XYL_{11} generally requires three unsubstituted Xyl*p* units [13,15].

Proposed structural models of wheat endosperm AX, based on enzymatic hydrolysis and periodate oxidation studies, suggest a non-random distribution of Ara*f* substituents along the Xyl*p* backbone [33,34]. According to these models, wheat AX can be broadly divided into regions of high and low substitution density. In highly substituted regions, clusters of one to three consecutively substituted Xyl*p* residues are proposed to occur, often followed by an unsubstituted Xyl*p* unit. With increasing substitution density, a corresponding increase in the release of AXOS containing doubly substituted Xyl*p* residues is observed, accompanied by a decrease in AXOS structures with monosubstituted Xyl*p* units. These findings are consistent with the results presented in this study. Overall, the (A)XOS profiles suggest that disubstitution is favored within the highly substituted domains of wheat AX.

Consistent with their close phylogenetic relationship, the additionally analyzed wheat species exhibited (A)XOS profiles that largely resembled those of common wheat, with SDF from emmer representing the main exception. Just as observed for wheat, XOS were enriched in the IDF fractions, most prominently in the XYL_{11} hydrolysates of emmer and spelt, where the total proportion of XOS exceeded 80 mol%. In contrast, AXOS predominated in the SDF hydrolysates. AXOS consisting exclusively of doubly substituted Xyl*p* units were released in comparatively high amounts. In the XYL_{11} hydrolysate of emmer SDF, $XA^{2+3}XX$ represented the dominant AXOS with a molar proportion of 33.3 mol%. The XYL_{10} hydrolysate of emmer SDF further contained considerable amounts of AXOS carrying two doubly substituted Xyl*p* units, accounting for 16.1 mol%. Fig. 3 shows the HPAEC-PAD chromatograms of (A)XOS released from emmer IDF and SDF after separate enzymatic hydrolysis with either XYL_{10} or XYL_{11}, Corresponding HPAEC-PAD chromatograms of the other wheat species are provided in Supplementary Fig. 4. Using the profiling method, important insights into the fine structure of the AX of these wheat species were obtained, which have so far been insufficiently described in the literature.

The profiling method was also applied to the analysis of other cereal genera such as rye (*Secale cereale* L.) and barley (*Hordeum vulgare* L.) (see Supplementary Fig. 5 for the corresponding HPAEC-PAD chromatograms). In the XYL_{11} hydrolysates of rye dietary fiber, XA^3XX represents the predominant AXOS, reaching molar proportions of 15.3 mol% in the IDF and 45.2 mol% in the SDF. The corresponding structures A^3X and XA^3X are also present after enzymatic digestion with XYL_{10} in comparatively high amounts, accounting for 8.9 and 9.3 mol% in the IDF, and 15.5 and 13.5 mol% in the SDF, respectively. In the SDF hydrolysates produced by both enzymes used individually, AXOS structures containing consecutive *O*3-monosubstituted Xyl*p* residues were additionally detected. While XYL_{10} released both XA^3A^3X and A^3A^3X with a combined molar proportion of 24.0 mol%, only XA^3A^3X (6.5 mol%) was identified in the XYL_{11} hydrolysate. In contrast, barley exhibits an AX structure that differs markedly from those of wheat and rye. A notable observation is that the total amount of AXOS released from the barley IDF exceeds the corresponding XOS fraction for both XYL_{10} (67.8 mol%) and XYL_{11} (50.8 mol%), indicating that unsubstituted Xyl*p* units are comparatively scarce in the enzymatically accessible region. Small amounts of A^2XX were detected in the XYL_{10} hydrolysates of barley IDF and SDF (2.6 mol% and 4.7 mol%, respectively). It cannot be excluded that XYL_{10} or XYL_{11} release additional *O*2-substituted AXOS that are not captured by the current profiling approach. Previous studies have also

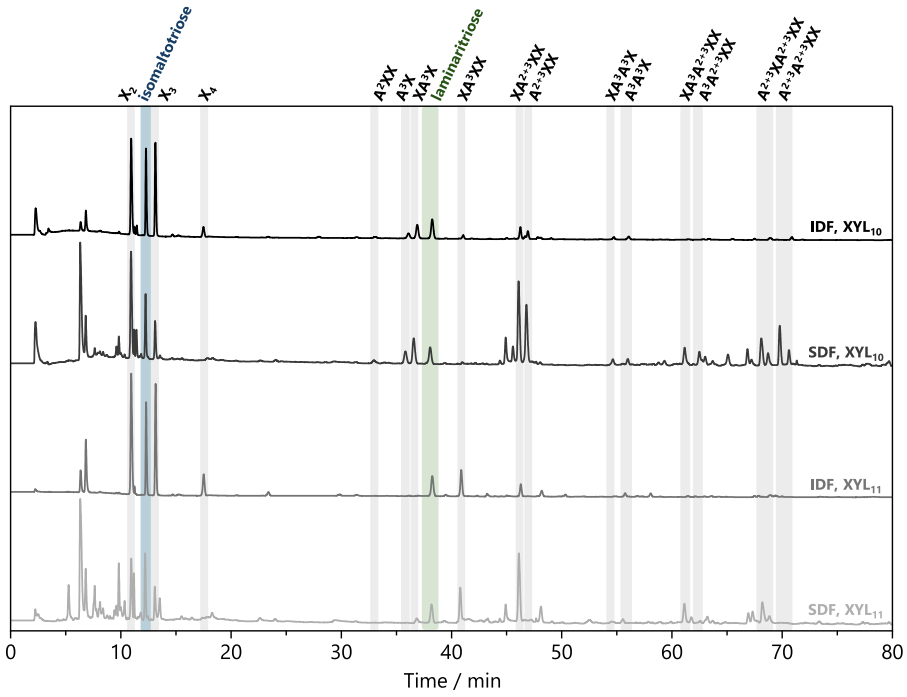

Fig. 3. PAD detected HPAEC chromatograms of (arabino-)xylooligosaccharides ((A)XOS) from insoluble and soluble dietary fiber (IDF, SDF) in emmer wheat following separate enzymatic hydrolysis with *endo*-β-1,4-xylanases of glycoside hydrolase families 10 (XYL_{10}) and 11 (XYL_{11}). (A)XOS are designated according to the naming system of Fauré et al. [14].

shown that *O*2-substituted Xyl*p* residues are mainly located in enzymatically resistant regions of barley AX and may therefore be inaccessible to hydrolysis by XYL_{10} or XYL_{11} [35]. Except for the XYL_{11} hydrolysate of the barley IDF, where XA^3XX is the dominant component (27.2 mol%), the released AXOS fractions generally show an increased presence of structures containing doubly substituted Xyl*p* units.

3.4. Comparison with carbohydrate conventional methods

Using *endo*-β-1,4-xylanases (XYL_{10} and XYL_{11}) in combination with sensitive and selective HPAEC-PAD/MS analysis enables a more detailed profiling of the fine structure of AX than routine methods based solely on monosaccharide composition and/or linkage analysis. In order to compare the monosaccharide compositions of IDF and SDF fractions obtained after acid hydrolysis with those derived from enzymatic hydrolyses, the corresponding arabinose-to-xylose ratios (A/X) were evaluated for both approaches. The A/X after enzymatic hydrolysis with XYL_{10} and XYL_{11}, respectively, were calculated from the amounts of Ara*f* and Xyl*p* residues present in the released (A)XOS and their respective proportions in the hydrolysate (see Table 4). For comparison, the A/X determined by monosaccharide analysis after acid hydrolysis are also reported in Table 4 (see Supplementary Tables 3–4 for complete monosaccharide compositions of cereal samples). The A/X ratios obtained from monosaccharide analysis were in good agreement with

Table 4
Arabinose-to-xylose ratios of arabinoxylans from insoluble and soluble dietary fiber fractions (IDF, SDF) of the investigated cereal species after acidic hydrolysis[a] (A/X_A, n = 3) and enzymatic hydrolysis[b] (A/X_E, n = 2) using *endo*-β-1,4-xylanases from glycoside hydrolase families 10 (XYL_{10}) and 11 (XYL_{11}). In addition, the data includes the relative abundances (mol%, n = 2) of partially methylated alditol acetates (PMAAs) of Xyl*p* residues[c] as determined by methylation analysis.

1			wheat	rye	einkorn	emmer	kamut	spelt	barley
IDF	A/X_A		0.60	0.53	0.55	0.54	0.62	0.51	0.70
	A/X_E	XYL_{10}	0.19	0.18	0.23	0.18	0.25	0.24	0.44
		XYL_{11}	0.11	0.09	0.10	0.08	0.11	0.10	0.26
	t-Xyl*p*		3.9	5.7	4.8	4.0	4.5	4.6	4.9
	1,4-Xyl*p*		68.5	63.6	63.3	66.7	62.4	62.4	50.3
	1,2,4-Xyl*p*		2.5	2.3	2.8	2.6	3.0	2.7	5.6
	1,3,4-Xyl*p*		12.8	16.4	13.6	12.6	14.3	14.3	12.0
	1,2,3,4-Xyl*p*		12.4	12.2	15.5	14.1	15.8	16.0	27.2
SDF	A/X_A		0.65	0.52	0.79	1.16	0.79	0.91	0.65
	A/X_E	XYL_{10}	0.43	0.46	0.47	0.53	0.46	0.42	0.50
		XYL_{11}	0.28	0.27	0.30	0.34	0.34	0.33	0.37
	t-Xyl*p*		2.5	1.3	3.4	2.6	3.0	2.5	2.1
	1,4-Xyl*p*		65.7	50.2	59.1	56.0	60.4	67.7	58.7
	1,2,4-Xyl*p*		1.7	2.0	1.7	2.7	2.2	2.1	3.7
	1,3,4-Xyl*p*		10.2	31.5	12.5	8.8	11.2	9.8	7.5
	1,2,3,4-Xyl*p*		19.9	15.0	23.3	29.8	23.2	17.9	28.1

[a] Calculated from the monosaccharide composition of IDF and SDF (see Supplementary Table 3–4).
[b] Calculated from the molar amounts of arabinofuranose and Xyl*p* residues in the enzymatically released (arabino-)xylooligosaccharides.
[c] Calculated as the molar percentage of the total quantified PMAAs derived from Xyl*p* residues (see Supplementary Tables 5–6). Total sum may not equal 100 % because of rounding.

literature values reported for AX from various wheat varieties, as well as from rye and barley [36,37]. In general, the A/X values derived from enzymatically released (A)XOS are lower than those obtained after acid hydrolysis. This indicates that a substantial fraction of AX in the different cereal samples is not fully represented by the profiling approach. While the enzymatic accessibility of AX in the SDF fraction mainly depends on the degree and pattern of substitution with Ara*f*, in the IDF fraction, the accessibility is likely additionally affected by AX cross-linking and interactions with other polysaccharides within the cell wall matrix. These structural interactions limit enzyme diffusion and obstruct access to cleavage sites, thereby decreasing the susceptibility of these regions to enzymatic hydrolysis. It should be noted, however, that arabinose released during acidic hydrolysis may also originate from other cell wall polysaccharides, such as arabinans and arabinogalactans. However, from a quantitative perspective, pectins play only a minor role in graminaceous cell walls compared with AX [3]. A comparison of the A/X values obtained with XYL_{10} and XYL_{11} shows consistently higher values for XYL_{10}. As discussed in section 3.3, XYL_{10} requires fewer consecutive unsubstituted Xyl*p* residues for cleavage, which allows it to access and hydrolyze more highly substituted regions of AX, thereby resulting in the release of more highly substituted AXOS.

Due to methodological differences, a direct comparison between methylation analysis and the enzymatic profiling approach is only possible to a limited extent. Methylation analysis provides information on the relative abundance of substitution positions across the entire AX structure. However, in contrast to the enzymatic approach applied here, it does not resolve the distribution pattern of Ara*f* substituents along the AX backbone, e.g. consecutive mono- or disubstituted Xyl*p* units cannot be identified. As noted above, the profiling method, however, does not fully capture highly substituted regions of AX. Nevertheless, data from both methods can be combined to identify trends in specific structural elements. Table 4 presents the molar percentage of the total quantified PMAAs derived from Xyl*p* residues in the different cereal samples (see Supplementary Tables 5–6 for complete PMAA compositions of cereal samples). AX from cereal IDF are typically supposed to contain a higher proportion of unsubstituted Xyl*p* units. This promotes aggregation and stronger interactions with cellulose microfibrils, thereby reducing their water solubility. However, this is not the case for spelt and barley, which contain a higher proportion of unsubstituted Xyl*p* units in water-soluble AX, while the proportions of mono- and disubstituted Xyl*p* units are comparable to those in water-insoluble AX. The water solubility of AX is therefore determined less by the absolute number of Ara*f* substituents and more by their distribution along the AX backbone, as well as by the presence of unsubstituted Xyl*p* units [4]. In addition to the arabinose substitution pattern, molecular weight and the presence of ferulic acid cross-links also have a decisive influence on the water solubility of AX [38,39]. Direct comparison of the proportions of terminal Xyl*p* units and unsubstituted 1,4-linked Xyl*p* residues with the (A)XOS profiles obtained by the profiling method is not appropriate. This is because enzymatic hydrolysis preferentially targets less heavily substituted regions of AX, resulting in (A)XOS that are relatively enriched in unsubstituted Xyl*p* units and consequently exhibit low A/X (see Table 4). In addition, both XYL_{10} and XYL_{11} generate (A)XOS with unsubstituted non-reducing ends, further contributing to a high proportion of terminal Xyl*p* units observed in enzymatic hydrolysates. Nonetheless, both enzymatically released AXOS and methylation analysis provide insights into the dominant substitution positions of backbone Xyl*p* units with Ara*f* residues. For example, the high levels of *O*3-monosubstitution in rye SDF (31.5 mol%) and disubstitution in emmer and barley SDF (29.8 and 28.1 mol%, respectively) are likewise reflected in the composition of the enzymatically released AXOS. Conclusively, the profiling method specifically enables detailed insights into the distribution of Ara*f* substituents along the AX backbone, as well as the occurrence of consecutive substituted and unsubstituted regions, but only covers enzymatically accessible regions. Thus, the two approaches should therefore be considered complementary, providing different but mutually informative perspectives on AX structure.

The results demonstrate that the HPAEC-PAD/MS profiling approach provides a powerful tool for elucidating the structural characteristics of enzymatically accessible AX from different cereal sources. Beyond plant-related applications, the developed profiling approach may also be applied to investigate structural changes in AX during food processing. For instance, during malt production, enzymatic degradation of water-soluble AX from barley grains results in a reduction in molecular weight, accompanied by changes in substitution patterns that can be effectively monitored using this method [40]. Similarly, the developed profiling approach may be applied to characterize the (A)XOS generated during breadmaking following the addition of *endo*-β-1,4-xylanases. Monitoring changes in the oligosaccharide profile would provide detailed insights into enzyme-induced AX depolymerization and could contribute to a better understanding of how different AX degradation products relate to dough functionality and bread quality [41].

4. Conclusion

Using commercially available and isolated (A)XOS standard compounds, an advanced HPAEC-PAD/MS-based profiling method was developed that enables both efficient separation and semi-quantitative determination of AX-derived oligosaccharides based on RRF. Through enzymatic hydrolysis of IDF and SDF fractions from various cereal grains, including different wheat (*Triticum*) species as well as other cereal genera, such as rye (*Secale cereale*) and barley (*Hordeum vulgare*), (A)XOS were released using *endo*-β-1,4-xylanases and subsequently analyzed by HPAEC-PAD. Coupling with MS further allowed the determination of molecular masses, supporting, in combination with RRT, reliable analyte identification and the detection of previously uncharacterized compounds. The resulting (A)XOS profiles provided detailed information on the position and distribution of Ara*f* substituents in AX. Additionally, the findings were in good agreement with those obtained using established conventional methods for structural characterization of cereal AX, but provided additional structural information. Thus, the developed HPAEC-PAD/MS profiling method provides a basis for a more comprehensive understanding of the structural diversity of cereal cell wall AX.

CRediT authorship contribution statement

Lukas Sitter: Data curation, Investigation, Methodology, Visualization, Writing – original draft, Writing – review & editing. **Mirko Bunzel:** Conceptualization, Methodology, Resources, Supervision, Writing – review & editing.

Declaration of competing interests

The authors declare that they have no known competing financial interests or personal relationships that could have appeared to influence the work reported in this paper.

Appendix A. Supplementary data

Supplementary data to this article can be found online at https://doi.org/10.1016/j.carres.2026.110074.

Data availability

Data will be made available on request.

References

[1] P.B. Mellen, T.F. Walsh, D.M. Herrington, Whole grain intake and cardiovascular disease: a meta-analysis, Nutr. Metabol. Cardiovasc. Dis. 18 (2008) 283–290, https://doi.org/10.1016/j.numecd.2006.12.008.

[2] E.Q. Ye, S.A. Chacko, E.L. Chou, M. Kugizaki, S. Liu, Greater whole-grain intake is associated with lower risk of type 2 diabetes, cardiovascular disease, and weight gain, J. Nutr. 142 (2012) 1304–1313, https://doi.org/10.3945/jn.113.179473.
[3] J. Vogel, Unique aspects of the grass cell wall, Curr. Opin. Plant Biol. 11 (2008) 301–307, https://doi.org/10.1016/j.pbi.2008.03.002.
[4] T. Köhnke, Å. Östlund, H. Brelid, Adsorption of arabinoxylan on cellulosic surfaces: influence of degree of substitution and substitution pattern on adsorption characteristics, Biomacromolecules 12 (2011) 2633–2641, https://doi.org/10.1021/bm200437m.
[5] M. Bunzel, Chemistry and occurrence of hydroxycinnamate oligomers, Phytochem. Rev. 9 (2010) 47–64, https://doi.org/10.1007/s11101-009-9139-3.
[6] C.M. Courtin, K. Swennen, W.F. Broekaert, Q. Swennen, J. Buyse, E. Decuypere, C. W. Michiels, B. De Ketelaere, J.A. Delcour, Effects of dietary inclusion of xylooligosaccharides, arabinoxylooligosaccharides and soluble arabinoxylan on the microbial composition of caecal contents of chickens, J. Sci. Food Agric. 88 (2008) 2517–2522, https://doi.org/10.1002/jsfa.3.
[7] J. Pan, J. Yin, K. Zhang, P. Xie, H. Ding, X. Huang, F. Blachier, X. Kong, Dietary xylooligosaccharide supplementation alters gut microbial composition and activity in pigs according to age and dose, AMB Express 9 (2019) 134, https://doi.org/10.1186/s13568-019-0858-6.
[8] A. Benítez-Páez, L. Kjølbæk, E.M.G.d. Pulgar, L.K. Brahe, A. Astrup, S. Matysik, H.-F. Schött, S. Krautbauer, G. Liebisch, J. Boberska, S. Claus, S. Rampelli, P. Brigidi, L.H. Larsen, Y. Sanz, A multi-omics approach to unraveling the microbiome-mediated effects of arabinoxylan oligosaccharides in overweight humans, mSystems 4 (2019) 1–16, https://doi.org/10.1128/msystems.00209-19.
[9] B. Damen, L. Cloetens, W.F. Broekaert, I. Francois, O. Lescroart, I. Trogh, F. Arnaut, G.W. Welling, J. Wijffels, J.A. Delcour, K. Verbeke, C.M. Courtin, Consumption of breads containing in situ-produced arabinoxylan oligosaccharides alters gastrointestinal effects in healthy volunteers, J. Nutr. 142 (2012) 470–477, https://doi.org/10.3945/jn.111.146464.
[10] C. Davies, G. González-Ortiz, T. Rinttilä, J. Apajalahti, M. Alyassin, M.R. Bedford, Stimbiotic supplementation and xylose-rich carbohydrates modulate broiler's capacity to ferment fibre, Front. Microbiol. 14 (2024), https://doi.org/10.3389/fmicb.2023.1301727.
[11] B.V. McCleary, V.A. McKie, A. Draga, E. Rooney, D. Mangan, J. Larkin, Hydrolysis of wheat flour arabinoxylan, acid-debranched wheat flour arabinoxylan and arabinoxylooligosaccharides by β-xylanase, α-L-arabinofuranosidase and β-xylosidase, Carbohydr. Res. 407 (2015) 79–96, https://doi.org/10.1016/j.carres.2015.01.017.
[12] H. Gruppen, R.A. Hoffmaann, F.J.M. Kormelink, A.G.J. Voragen, J.P. Kamerlin, J.F. G. Vliegenthart, Characterisation by ^{1}H NMR spectroscopy of enzymically derived oligosaccharides from alkali-extractable wheat-flour arabinoxylan, Carbohydr. Res. 233 (1992) 45–64, https://doi.org/10.1016/S0008-6215(00)90919-4.
[13] P. Biely, S. Singh, V. Puchart, Towards enzymatic breakdown of complex plant xylan structures: state of the art, Biotechnol. Adv. 34 (2016) 1260–1274, https://doi.org/10.1016/j.biotechadv.2016.09.001.
[14] R. Fauré, C.M. Courtin, J.A. Delcour, C. Dumon, C.B. Faulds, G.B. Fincher, S. Fort, S.C. Fry, S. Halila, M.A. Kabel, L. Pouvreau, B. Quemener, A. Rivet, L. Saulnier, H. A. Schols, H. Driguez, M.J. O'Donohue, A brief and informationally rich naming system for oligosaccharide motifs of heteroxylans found in plant cell walls, Aust. J. Chem. 62 (2009) 533–537, https://doi.org/10.1071/CH08458.
[15] A. Pollet, J.A. Delcour, C.M. Courtin, Structural determinants of the substrate specificities of xylanases from different glycoside hydrolase families, Crit. Rev. Biotechnol. 30 (2010) 176–191, https://doi.org/10.3109/07388551003645599.
[16] M.A. Correia, K. Mazumder, J.L. Brás, S.J. Firbank, Y. Zhu, R.J. Lewis, W.S. York, C.M. Fontes, H.J. Gilbert, Structure and function of an arabinoxylan-specific xylanase, J. Biol. Chem. 286 (2011) 22510–22520, https://doi.org/10.1074/jbc.M110.217315.
[17] A. Rivière, S. Eeltink, C. Pierlot, T. Balzarini, F. Moens, M. Selak, L. De Vuyst, Development of an ion-exchange chromatography method for monitoring the degradation of prebiotic arabinoxylan-oligosaccharides in a complex fermentation medium, Anal. Chem. 85 (2013) 4982–4990, https://doi.org/10.1021/ac400187f.
[18] G.E. Joyce, I.A. Kagan, M.D. Flythe, B.E. Davis, R.R. Schendel, Profiling of cool-season forage arabinoxylans via a validated HPAEC-PAD method, Front. Plant Sci. 14 (2023) 1–13, https://doi.org/10.3389/fpls.2023.1116995.
[19] M. Alyassin, G.M. Campbell, H. Masey O'Neill, M.R. Bedford, Simultaneous determination of cereal monosaccharides, xylo- and arabinoxylo-oligosaccharides and uronic acids using HPAEC-PAD, Food Chem. 315 (2020) 126221, https://doi.org/10.1016/j.foodchem.2020.126221.
[20] L. Sitter, M. Bunzel, 2D-NMR characterization of higher substituted oligosaccharides isolated from enzymatic wheat flour arabinoxylan hydrolysates, Front. Plant Sci. 17 (2026) 1–15, https://doi.org/10.3389/fpls.2026.1784230.
[21] M. Bunzel, J. Ralph, J.M. Marita, R.D. Hatfield, H. Steinhart, Diferulates as structural components in soluble and insoluble cereal dietary fibre, J. Sci. Food Agric. 81 (2001) 653–660, https://doi.org/10.1002/jsfa.861.
[22] J.F. Saeman, J.L. Bubl, E.E. Harris, Quantitative saccharification of wood and cellulose, Ind. Eng. Chem. Anal. Ed. 17 (1945) 35–37, https://doi.org/10.1021/i560137a008.
[23] S. Willför, A. Pranovich, T. Tamminen, J. Puls, C. Laine, A. Suurnäkki, B. Saake, K. Uotila, H. Simolin, J. Hemming, B. Holmbom, Carbohydrate analysis of plant materials with uronic acid-containing polysaccharides–A comparison between different hydrolysis and subsequent chromatographic analytical techniques, Ind. Crop. Prod. 29 (2009) 571–580, https://doi.org/10.1016/j.indcrop.2008.11.003.
[24] G.A. De Ruiter, H.A. Schols, A.G.J. Voragen, F.M. Rombouts, Carbohydrate analysis of water-soluble uronic acid-containing polysaccharides with high-performance anion-exchange chromatography using methanolysis combined with TFA hydrolysis is superior to four other methods, Anal. Biochem. 207 (1992) 176–185, https://doi.org/10.1016/0003-2697(92)90520-H.
[25] R.R. Schendel, A. Becker, C.E. Tyl, M. Bunzel, Isolation and characterization of feruloylated arabinoxylan oligosaccharides from the perennial cereal grain intermediate wheat grass (*Thinopyrum intermedium*), Carbohydr. Res. 407 (2015) 16–25, https://doi.org/10.1016/j.carres.2015.01.006.
[26] D.P. Sweet, R.H. Shapiro, P. Albersheim, Quantitative analysis by various g.l.c response-factor theories for partially methylated and partially ethylated alditol acetates, Carbohydr. Res. 40 (1975) 217–225, https://doi.org/10.1016/S0008-6215(00)82604-X.
[27] T. Rundlöf, I. McEwen, M. Johansson, T. Arvidsson, Use and qualification of primary and secondary standards employed in quantitative ^{1}H NMR spectroscopy of pharmaceuticals, J. Pharm. Biomed. Anal. 93 (2014) 111–117, https://doi.org/10.1016/j.jpba.2013.09.010.
[28] A. Bhattacharya, A. Ruthes, F. Vilaplana, E.N. Karlsson, P. Adlecreutz, H. Stålbrand, Enzyme synergy for the production of arabinoxylooligosaccharides from highly substituted arabinoxylan and evaluation of their prebiotic potential, LWT Food Sci. Technol. 131 (2020) 109762, https://doi.org/10.1016/j.lwt.2020.109762.
[29] S. Mathew, E.N. Karlsson, P. Adlercreutz, Extraction of soluble arabinoxylan from enzymatically pretreated wheat bran and production of short xylo-oligosaccharides and arabinoxylo-oligosaccharides from arabinoxylan by glycoside hydrolase family 10 and 11 endoxylanases, J. Biotechnol. 260 (2017) 53–61, https://doi.org/10.1016/j.jbiotec.2017.09.006.
[30] G. Henriksson, U. Germgård, M.E. Lindström, A review on chemical mechanisms of kraft pulping, Nord. Pulp Pap Res. J. 39 (2024) 297–311, https://doi.org/10.1515/npprj-2023-0015.
[31] J. Steck, L. Kaufhold, M. Bunzel, Structural profiling of xyloglucans from food plants by high-performance anion-exchange chromatography with parallel pulsed amperometric and mass spectrometric detection, J. Agric. Food Chem. 69 (2021) 8838–8849, https://doi.org/10.1021/acs.jafc.1c02967.
[32] D. Wefers, M. Bunzel, Arabinan and galactan oligosaccharide profiling by high-performance anion-exchange chromatography with pulsed amperometric detection (HPAEC-PAD), J. Agric. Food Chem. 64 (2016) 4656–4664, https://doi.org/10.1021/acs.jafc.6b01121.
[33] G. Dervilly-Pinel, V. Tran, L. Saulnier, Investigation of the distribution of arabinose residues on the xylan backbone of water-soluble arabinoxylans from wheat flour, Carbohydr. Polym. 55 (2004) 171–177, https://doi.org/10.1016/j.carbpol.2003.09.004.
[34] H. Gruppen, F.J.M. Kormelink, A.G.J. Voragen, Water-unextractable cell wall material from wheat flour. 3. A structural model for arabinoxylans, J. Cereal. Sci. 18 (1993) 111–128, https://doi.org/10.1006/jcrs.1993.1040.
[35] R.J. Viëtor, F.J.M. Kormelink, S.A.G.F. Angelino, A.G.J. Voragen, Substitution patterns of water-unextractable arabinoxylans from barley and malt, Carbohydr. Polym. 24 (1994) 113–118, https://doi.org/10.1016/0144-8617(94)90020-5.
[36] K. Gebruers, E. Dornez, D. Boros, A. Fraś, W. Dynkowska, Z. Bedő, M. Rakszegi, J. A. Delcour, C.M. Courtin, Variation in the content of dietary fiber and components thereof in wheats in the HEALTHGRAIN diversity screen, J. Agric. Food Chem. 56 (2008) 9740–9749, https://doi.org/10.1021/jf800975w.
[37] G. Dervilly-Pinel, L. Rimsten, L. Saulnier, R. Andersson, P. Åman, Water-extractable arabinoxylan from pearled flours of wheat, barley, rye and triticale. Evidence for the presence of ferulic acid dimers and their involvement in gel formation, J. Cereal. Sci. 34 (2001) 207–214, https://doi.org/10.1006/jcrs.2001.0392.
[38] C. Maes, J.A. Delcour, Structural characterisation of water-extractable and water-unextractable arabinoxylans in wheat bran, J. Cereal. Sci. 35 (2002) 315–326, https://doi.org/10.1006/jcrs.2001.0439.
[39] L. Saulnier, P.-E. Sado, G. Branlard, G. Charmet, F. Guillon, Wheat arabinoxylans: exploiting variation in amount and composition to develop enhanced varieties, J. Cereal. Sci. 46 (2007) 261–281, https://doi.org/10.1016/j.jcs.2007.06.014.
[40] P. Michiels, W. Debyser, N.A. Langenaeken, C.M. Courtin, Impact of barley selection and mashing profile on the arabinoxylan content and structure in beer, Int. J. Biol. Macromol. 280 (2024) 136031, https://doi.org/10.1016/j.ijbiomac.2024.136031.
[41] X.-N. Guo, S. Yang, K.-X. Zhu, Impact of arabinoxylan with different molecular weight on the thermo-mechanical, rheological, water mobility and microstructural characteristics of wheat dough, Int. J. Food Sci. Technol. 53 (2018) 2150–2158, https://doi.org/10.1111/ijfs.13802.